

Title	[10]B+ states with chain-like structures in [14]N
Author(s)	Kanada-En'yo, Yoshiko
Citation	Physical Review C - Nuclear Physics (2015), 92(6)
Issue Date	2015-12-30
URL	<a href="http://hdl.handle.net/2433/218370">http://hdl.handle.net/2433/218370</a>
Right	© 2015 American Physical Society.
Type	Journal Article
Textversion	publisher

**$^{10}\text{B} + \alpha$  states with chain-like structures in  $^{14}\text{N}$** 

Yoshiko Kanada-En'yo

*Department of Physics, Kyoto University, Kyoto 606-8502, Japan*

(Received 20 May 2015; revised manuscript received 11 September 2015; published 30 December 2015)

I investigate  $^{10}\text{B} + \alpha$ -cluster states of  $^{14}\text{N}$  with a  $^{10}\text{B} + \alpha$ -cluster model. Near the  $\alpha$ -decay threshold energy, I obtain  $K^\pi = 3^+$  and  $K^\pi = 1^+$  rotational bands having  $^{10}\text{B}(3^+) + \alpha$  and  $^{10}\text{B}(1^+) + \alpha$  components, respectively. I assign the bandhead state of the  $K^\pi = 3^+$  band to the experimental  $3^+$  at  $E_x = 13.19$  MeV of  $^{14}\text{N}$  observed in  $\alpha$  scattering reactions by  $^{10}\text{B}$  and show that the calculated  $\alpha$ -decay width is consistent with the experimental data. I discuss an  $\alpha$ -cluster motion around the  $^{10}\text{B}$  cluster and show that the  $K^\pi = 3^+$  and  $K^\pi = 1^+$  rotational bands contain an enhanced component of a linear-chain  $3\alpha$  configuration, in which an  $\alpha$  cluster is localized in the longitudinal direction around the deformed  $^{10}\text{B}$  cluster.

DOI: [10.1103/PhysRevC.92.064326](https://doi.org/10.1103/PhysRevC.92.064326)

PACS number(s): 27.20.+n, 21.10.Tg, 21.60.Gx

**I. INTRODUCTION**

It is known that cluster structures appear in various nuclei including unstable nuclei (for instance, Refs. [1–5] and references therein). For cluster states having an  $\alpha$  cluster around a core nucleus, well-known examples are  $^{16}\text{O} + \alpha$  states in  $^{20}\text{Ne}$  and  $^{12}\text{C} + \alpha$  states in  $^{16}\text{O}$  [6]. Recent experimental and theoretical studies have revealed many cluster resonances in highly excited states near the  $\alpha$ -decay threshold also in unstable nuclei, for instance,  $A-4\text{He} + \alpha$  states in Be isotopes [1,4,7–26],  $^{10}\text{Be} + \alpha$  states in  $^{14}\text{C}$  [27–31],  $^{14}\text{C} + \alpha$  states in  $^{18}\text{O}$  and their mirror states [32–41], and  $^{18}\text{O} + \alpha$  states in  $^{22}\text{Ne}$  [39–46].

Multi- $\alpha$ -cluster states such as cluster gas and linear-chain states of  $n\alpha$  systems are also interesting topics. The  $\alpha$ -cluster gas was proposed by Tohsaki *et al.* to describe the  $3\alpha$ -cluster structure of  $^{12}\text{C}(0_2^+)$  [47] and extended to excited states of  $^{12}\text{C}$  and other nuclei [48–50]. The linear-chain  $n\alpha$  state was originally proposed for  $^{12}\text{C}(0_2^+)$  by Morinaga in the 1950s and 1960s [51,52]. However, in the 1970s, this picture was excluded at least for  $^{12}\text{C}(0_2^+)$  having a larger  $\alpha$ -decay width than the one expected from the linear-chain structure [53]. Despite many discussions for several decades, the existence of linear-chain  $n\alpha$  states has not yet been confirmed and it is still an open problem to be solved. It is naively expected that the linear-chain configuration is not favored in an  $n\alpha$  system because it costs much kinetic energy to keep  $\alpha$  clusters in a row. This means that some mechanism is necessary to form the linear-chain structure. In the 1990s and 2000s, it was proposed for neutron-rich C isotopes that excess neutrons may stabilize the linear-chain structure [1,8]. Itagaki *et al.* analyzed the stability of a  $3\alpha$ -chain configuration surrounded by excess neutrons in molecular orbitals against the bending motion and suggested that the linear-chain structure can be stable in  $^{16}\text{C}$  but unstable in  $^{12}\text{C}$  and  $^{14}\text{C}$  [54]. More recently, Suhara and I predicted a rotational band with a linear  $3\alpha$ -chain configuration in excited states of  $^{14}\text{C}$  near the  $\alpha$ -decay threshold [31]. They pointed out that the orthogonal condition to lower states is important for the stability of the linear-chain structure. The linear-chain structure is expected to be more favored in high-spin states because of the stretching effect in rotating systems as suggested in  $^{15}\text{C}$  [1] and  $^{16}\text{O}$  [55].

According to analysis in Refs. [31,56], linear-chain states of  $^{14}\text{C}$  are found to have a  $2\alpha + 2n$  correlation and are

interpreted as  $^{10}\text{Be} + \alpha$  structures, where the  $^{10}\text{Be}$  cluster is a prolately deformed state containing a  $2\alpha$  core and an additional  $\alpha$  cluster is located in the longitudinal direction of the  $^{10}\text{Be}$  cluster. Similarly, the linear-chain state of  $^{15}\text{C}$  suggested in Ref. [1] also shows a  $^{11}\text{Be} + \alpha$ -cluster structure with a prolately deformed  $^{11}\text{Be}$  cluster and an  $\alpha$  cluster in the longitudinal direction. This means that, the linear-chain states in these neutron-rich C tend to have the  $2\alpha$  correlation, and therefore  $3\alpha$  linear-chain structures are expected to be found in Be +  $\alpha$ -cluster states.

In this paper, I focus on  $^{10}\text{B} + \alpha$ -cluster states in excited states of  $^{14}\text{N}$ . In experimental energy levels of  $^{14}\text{N}$  near the  $\alpha$ -decay threshold,  $J^\pi = 3^+$  and  $1^+$  resonances were observed by  $\alpha$  elastic scattering by  $^{10}\text{B}$  [57]. These resonances are expected to be  $^{10}\text{B} + \alpha$ -cluster states because of significant  $\alpha$ -decay widths. In analogy to  $^{10}\text{Be} + \alpha$ -cluster states, it is interesting to investigate whether  $^{10}\text{B} + \alpha$ -cluster states with the dominant linear-chain structure exist. The ground state ( $3^+$ ) and the first excited state ( $1^+$ ) of  $^{10}\text{B}$  can be described by the deformed state with a  $2\alpha$  core surrounded by  $pn$  as discussed in Refs. [7,58]. If a  $^{10}\text{B} + \alpha$ -cluster state has an  $\alpha$  cluster in the longitudinal direction of the deformed  $^{10}\text{B}$  cluster, the  $^{10}\text{B} + \alpha$ -cluster state can be interpreted as a kind of linear-chain state that contains dominantly  $3\alpha$  clusters arranged in a row.

My aim is to study  $^{10}\text{B} + \alpha$ -cluster states of  $^{14}\text{N}$  near the threshold energy and discuss  $3\alpha$  configurations, in particular, the linear-chain component in the  $^{10}\text{B} + \alpha$ -cluster states. I calculate  $^{10}\text{B}(3^+) \otimes L_\alpha$  and  $^{10}\text{B}(1^+) \otimes L_\alpha$  components and evaluate partial  $\alpha$ -decay widths of  $^{10}\text{B} + \alpha$ -cluster states. To discuss stability of the linear-chain  $^{10}\text{B} + \alpha$  structure, I analyze the angular motion of an  $\alpha$  cluster around the deformed  $^{10}\text{B}$  cluster, i.e., rotation of the  $^{10}\text{B}$  cluster.

This paper is organized as follows. In Sec. II, I explain the formulation of the present  $^{10}\text{B} + \alpha$ -cluster model. In Sec. III, calculated positive-parity states and  $E2$  transition strengths of  $^{14}\text{N}$  are shown. I discuss  $\alpha$ -cluster motion around  $^{10}\text{B}(3^+)$  and  $^{10}\text{B}(1^+)$  in Sec. IV. Finally, a summary is given in Sec. V.

**II. FORMULATION OF THE  $^{10}\text{B} + \alpha$ -CLUSTER MODEL****A. Description of the  $^{10}\text{B}$  cluster**

For the  $^{10}\text{B}$  cluster in the present  $^{10}\text{B} + \alpha$ -cluster model, I adopt a  $2\alpha + (pn)$  wave function which can reasonably de-

scribe features of the ground ( $J^\pi = 3^+$ ) and first excited ( $1^+$ ) states of  $^{10}\text{B}$  as discussed in Ref. [58]. The  $2\alpha + (pn)$  wave function is given by a three-body cluster wave function, where  $\alpha$  clusters and a dinucleon ( $pn$ ) cluster are written by  $(0s)^4$  and  $(0s)^2$  harmonic oscillator configurations, respectively, as

$$\Phi_{2\alpha+pn}(\mathbf{R}_1, \mathbf{R}_2, \mathbf{R}_3) = \mathcal{A}\{\Phi_\alpha(\mathbf{R}_1)\Phi_\alpha(\mathbf{R}_2)\Phi_{pn}(\mathbf{R}_3)\}, \quad (1)$$

$$\Phi_\alpha(\mathbf{R}) = \psi_{p\uparrow}(\mathbf{R})\psi_{p\downarrow}(\mathbf{R})\psi_{n\uparrow}(\mathbf{R})\psi_{n\downarrow}(\mathbf{R}), \quad (2)$$

$$\Phi_{pn}(\mathbf{R}) = \psi_{p\uparrow}(\mathbf{R})\psi_{n\uparrow}(\mathbf{R}), \quad (3)$$

$$\psi_\sigma(\mathbf{R}) = \varphi_{0s}(\mathbf{R})\chi_\sigma, \quad (4)$$

where  $\mathcal{A}$  is the antisymmetrizer for all nucleons,  $\varphi_{0s}(\mathbf{R})$  is the spatial part of the single-particle wave function of the  $0s$  orbit around  $\mathbf{R}$ ,

$$\varphi_{0s}(\mathbf{R}) = \left(\frac{2\nu}{\pi}\right)^{3/4} \exp\{-\nu(\mathbf{r} - \mathbf{R})^2\}, \quad (5)$$

and  $\chi_\sigma$  is the spin-isospin wave function for  $\sigma = p\uparrow, p\downarrow, n\uparrow$ , and  $n\downarrow$ . For the  $^{10}\text{B}$  cluster, I set two  $\alpha$  clusters in the  $z$  direction as  $\mathbf{R}_1 - \mathbf{R}_2 = (0, 0, d_{2\alpha})$  with  $d_{2\alpha} = 3$  fm and a spin-aligned  $pn$  cluster on the  $x$ - $y$  plane at the distance  $d$  from the  $2\alpha$  center as  $\mathbf{R}_3 - (\mathbf{R}_1 + \mathbf{R}_2)/2 = (d \cos \phi, d \sin \phi, 0)$ . I write the  $^{10}\text{B}$  wave function localized around  $\mathbf{X}_B \equiv (4\mathbf{R}_1 + 4\mathbf{R}_2 + 2\mathbf{R}_3)/10$  as  $\Phi_{^{10}\text{B}}(\mathbf{X}_B; d, \phi)$  with the center position  $\mathbf{X}_B$  and the distance and angle parameters,  $d$  and  $\phi$ , for the  $pn$ -cluster position. In the  $^{10}\text{B} + \alpha$ -cluster model, I superpose the  $^{10}\text{B}$  wave functions with  $d = 1$  and  $2$  (fm) and  $\phi_j = \frac{\pi}{4}(j - 0.5)$  ( $j = 1, \dots, 8$ ).

### B. $^{14}\text{N}$ wave function in the $^{10}\text{B} + \alpha$ model

A  $^{10}\text{B} + \alpha$  wave function is written using the  $^{10}\text{B}$  wave function  $\Phi_{^{10}\text{B}}(\mathbf{X}_B; d, \phi)$  and the  $\alpha$ -cluster wave function  $\Phi_\alpha(\mathbf{X}_\alpha)$  as

$$\Phi_{^{10}\text{B}+\alpha}(D_\alpha, \theta_\alpha; d, \phi) = \mathcal{A}\{\Phi_{^{10}\text{B}}(\mathbf{X}_B; d, \phi)\Phi_\alpha(\mathbf{X}_\alpha)\}, \quad (6)$$

where  $\mathbf{R}_\alpha \equiv \mathbf{X}_\alpha - \mathbf{X}_B$  is written as  $\mathbf{R}_\alpha = (D_\alpha \sin \theta_\alpha, 0, D_\alpha \cos \theta_\alpha)$ . The center-of-mass position is taken to be  $4\mathbf{X}_\alpha + 10\mathbf{X}_B = 0$  so as to decouple the center-of-mass motion and the intrinsic wave function. It should be commented that  $\Phi_{^{10}\text{B}+\alpha}(D_\alpha, \theta_\alpha; d, \phi)$  is equivalent to a Brink cluster model wave function [59] of three  $\alpha$  clusters and a deuteron cluster, which is a typical multicenter cluster wave function where clusters are localized around certain positions. In this wave function, the  $\alpha$ -cluster wave function relative to the  $^{10}\text{B}$  cluster is expressed by a localized Gaussian  $\exp[-\nu_\alpha(\mathbf{r} - \mathbf{R}_\alpha)^2]$  ( $\nu_\alpha = 20\nu/7$ ) with the center position  $\mathbf{R}_\alpha$ . This means that the parameters  $\mathbf{R}_\alpha$ , i.e., the parameters  $D_\alpha$  and  $\theta_\alpha$ , indicate the Gaussian center position and can be interpreted as an  $\alpha$ -cluster position though they are not classical coordinates in a strict meaning. Here,  $D_\alpha$  and  $\theta_\alpha$  are the distance and angle parameters of the  $\alpha$ -cluster position relative to the deformed  $^{10}\text{B}$  cluster (see Fig. 1).

Wave functions for the  $n$ th  $J^\pi$  states ( $J_n^\pi$ ) of  $^{14}\text{N}$  are expressed by superposition of the  $J^\pi$ -projected wave

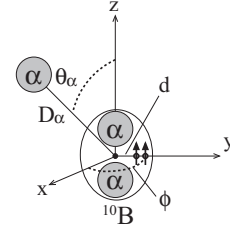


FIG. 1. Schematic figure for a  $^{10}\text{B} + \alpha$  configuration for the parameters in Eq. (6).

functions as

$$\Psi_{^{14}\text{N}(J_n^\pi)} = \sum_K \sum_{D_\alpha, \theta_\alpha} \sum_{d, \phi} C(K, D_\alpha, \theta_\alpha, d, \phi) \times \hat{P}_{MK}^{J_n^\pi} \Phi_{^{10}\text{B}+\alpha}(D_\alpha, \theta_\alpha; d, \phi), \quad (7)$$

where  $\hat{P}_{MK}^{J_n^\pi}$  is the parity and total angular momentum projection operator. Coefficients  $C(K, D_\alpha, \theta_\alpha, d, \phi)$  are determined by diagonalizing Hamiltonian and norm matrices. I take  $D_\alpha = \{2, \dots, 6\}$  (fm),  $\theta_\alpha = \{0, \pi/4, \pi/2, 3\pi/4, \pi\}$ ,  $d = \{1, 2\}$  (fm), and  $\phi = \frac{\pi}{4}(j - 0.5)$  ( $j = 1, \dots, 8$ ). In the practical calculation, the  $\theta_\alpha = 0 - \pi$  summation can be reduced to the  $\theta_\alpha = 0 - \pi/2$  summation because of the reflection symmetry of the  $^{10}\text{B}$  cluster. In the present paper, I calculate positive-parity ( $\pi = +$ ) states of  $^{14}\text{N}$ .

In Eq. (7), the  $\phi$  superposition is equivalent to the  $I_z$  mixing of the  $^{10}\text{B}$  cluster [ $I_z$  is the  $z$  component of the angular momentum (spin)  $\mathbf{I}$  of the  $^{10}\text{B}$  cluster]. The coupling of  $\mathbf{I}$  (the spin of the  $^{10}\text{B}$  cluster) and  $\mathbf{L}_\alpha$  (the orbital angular momentum of the  $\alpha$  cluster relative to the  $^{10}\text{B}$  cluster) is implicitly described by the  $J^\pi$  projection,  $K$  mixing, and  $\theta_\alpha$  and  $\phi$  summations.  $\mathbf{L}_\alpha$  couples with  $\mathbf{I}$  to the total angular momentum  $\mathbf{J} = \mathbf{L}_\alpha + \mathbf{I}$ . The  $z$  component,  $J_z = I_z + L_{\alpha z}$ , is the so-called  $K$  quantum, which takes  $K = -J, \dots, +J$ . Note that, in the present definition, the orientation of the aligned intrinsic spin of the  $pn$  cluster is chosen to be the  $+z$  direction as  $S_z = +1$ , and therefore  $K$  can be a negative value when the  $z$  component of the total orbital angular momentum is less than  $-1$ , meaning that the total orbital angular momentum is in the direction opposite to the intrinsic spin orientation. Strictly speaking,  $L_\alpha = 0, 2$  ( $S, D$ -wave) mixing is approximately taken into account by the summation of  $\theta_\alpha = \{0, \pi/4, \pi/2, 3\pi/4, \pi\}$  but higher  $L_\alpha (\geq 4)$  mixing cannot be controlled in the present calculation because of the finite number of mesh points for  $\theta_\alpha$ .

### C. Overlap function and $\alpha$ -cluster probability

To investigate  $^{10}\text{B} + \alpha$  components, I introduce specific  $^{10}\text{B} + \alpha$  wave functions for the  $\alpha$  cluster at a channel radius ( $D_\alpha$ ) and take their overlap with the  $^{14}\text{N}$  wave function [ $\Psi_{^{14}\text{N}(J_n^\pi)}$  in Eq. (7)]. In the present analysis, I mainly discuss the angular motion of the  $\alpha$  cluster around the  $^{10}\text{B}$  cluster using two kinds of  $^{10}\text{B} + \alpha$  wave functions based on the strong-coupling and weak-coupling pictures. One is the  $^{10}\text{B} + \alpha$  wave function having the  $\alpha$  cluster at a certain orientation  $\theta_\alpha$ . In this case, the state has a specific geometry and contains large mixing of  $L_\alpha$  eigen states, which corresponds to a so-called strong coupling state. The other is the  $^{10}\text{B} + \alpha$  wave function

having the  $\alpha$  cluster in an  $L_\alpha$  eigen state, which corresponds to a weak coupling state, where the angular momentum  $L_\alpha$  of the  $\alpha$  cluster weakly couples with the spin  $I^\pi$  of the  $^{10}\text{B}$  cluster.

**1. Overlap with specific geometric configurations based on the strong-coupling picture**

I consider the  $I_z^\pi$  projection for the  $^{10}\text{B}$  cluster of the  $^{10}\text{B} + \alpha$  wave function  $\Phi_{^{10}\text{B}+\alpha}(D_\alpha, \theta_\alpha; d, \phi)$  [defined in Eq. (6)] as

$$\Phi_{^{10}\text{B}(I_z^\pi)+\alpha}(D_\alpha, \theta_\alpha) = \sum_j c_j \Phi_{^{10}\text{B}+\alpha}(D_\alpha, \theta_\alpha; d = 2, \phi_j), \quad (8)$$

with  $c_j = \exp[i(I_z - 1)\phi_j]$ ,  $I_z = \{1, 3\}$ ,  $\pi = +$ , and  $\phi_j = \frac{\pi}{4}(j - 0.5)$  ( $j = 1, \dots, 8$ ).  $I_z$ , the  $z$  component of the total angular momentum  $I$  of  $^{10}\text{B}$ , is given by the sum of the  $z$  component of the intrinsic spin ( $S_z = +1$ ) and that ( $I_z - 1$ ) of the orbital angular momentum for the  $\phi$  rotation of the  $pn$  cluster. The  $I_z$  projection is approximately performed, whereas the parity  $\pi$  projection of  $^{10}\text{B}$  is exactly done because of the reflection symmetry of the  $^{10}\text{B}$  cluster. For simplicity, I fix  $d = 2$  fm in the present analysis.  $\Phi_{^{10}\text{B}(I_z^\pi)+\alpha}(D_\alpha, \theta_\alpha)$  in Eq. (8) stands for the wave function for the  $\alpha$  cluster at  $(D_\alpha, \theta_\alpha)$  around the  $I_z^\pi$ -projected  $^{10}\text{B}$  cluster.

I calculate the squared overlap of the  $JK$ -projected state  $\hat{P}_{MK}^{JK} \Phi_{^{10}\text{B}(I_z^\pi)+\alpha}(D_\alpha, \theta_\alpha)$  of  $\Phi_{^{10}\text{B}(I_z^\pi)+\alpha}(D_\alpha, \theta_\alpha)$  with the  $^{14}\text{N}$  wave function  $\Psi_{^{14}\text{N}(J_n^\pi)}$ ,

$$P[JK; ^{10}\text{B}(I_z^\pi); D_\alpha, \theta_\alpha] = \frac{|\langle \hat{P}_{MK}^{JK} \Phi_{^{10}\text{B}(I_z^\pi)+\alpha}(D_\alpha, \theta_\alpha) | \Psi_{^{14}\text{N}(J_n^\pi)} \rangle|^2}{\langle \hat{P}_{MK}^{JK} \Phi_{^{10}\text{B}(I_z^\pi)+\alpha}(D_\alpha, \theta_\alpha) | \hat{P}_{MK}^{JK} \Phi_{^{10}\text{B}(I_z^\pi)+\alpha}(D_\alpha, \theta_\alpha) \rangle}, \quad (9)$$

which indicates the  $\alpha$ -cluster probability at  $(D_\alpha, \theta_\alpha)$  around the  $I_z^\pi$ -projected  $^{10}\text{B}$  cluster. The probability  $P[JK; ^{10}\text{B}(I_z^\pi); D_\alpha, \theta_\alpha]$  is useful to analyze the  $\alpha$ -cluster motion and helpful to discuss geometric configurations of  $3\alpha$  clusters in  $^{10}\text{B} + \alpha$ -cluster states in the strong-coupling picture. For instance,  $P[JK; ^{10}\text{B}(I_z^\pi); D_\alpha, \theta_\alpha]$  for  $\theta_\alpha \sim 0$  means the component of the ‘‘longitudinal’’ configuration, where the  $\alpha$  cluster is localized in the longitudinal direction of the deformed  $^{10}\text{B}(I_z^\pi)$  cluster. This configuration corresponds to the linear-chain structure as three  $\alpha$  clusters are arranged in a row as shown in Fig. 2(b). For  $\theta_\alpha \sim \pi/2$ ,  $P[JK; ^{10}\text{B}(I_z^\pi); D_\alpha, \theta_\alpha]$  indicates the component of the ‘‘transverse configuration’’ for the  $\alpha$  cluster in the transverse direction of the deformed  $^{10}\text{B}(I_z^\pi)$  cluster [see Fig. 2(c)]. Schematic figures for angular momentum coupling of  $L_\alpha$ ,  $I$ , and  $J$  in the  $JK$ -projected state  $\hat{P}_{MK}^{JK} \Phi_{^{10}\text{B}(I_z^\pi)+\alpha}(D_\alpha, \theta_\alpha)$  for a given configuration  $D_\alpha, \theta_\alpha$  are shown in Fig. 2. Note that, in the  $JK$ -projected state,  $I_z$ ,  $L_{\alpha z}$ , and  $J$ , as well as  $K = I_z + L_{\alpha z}$ , are eigen values, but  $L_\alpha$  and  $I$  are not eigen values. This means that the state contains various  $L_\alpha$  and  $I$  states coupling to total  $J$  states. The longitudinal configuration contains only the  $K = I_z$  ( $L_{\alpha z} = 0$ ) component meaning that  $L_\alpha$  is always perpendicular to the  $z$  axis because of the axial symmetry. The transverse configuration contains  $K \neq I_z$  components as well as the  $K = I_z$  component. In particular, the  $JK$ -projected state for  $K > I_z$  corresponds to the alignment of  $L_\alpha$  to the  $z$  axis.

At a given channel radius  $D_\alpha$ ,  $P[JK; ^{10}\text{B}(I_z^\pi); D_\alpha, \theta_\alpha]$  shows the  $\theta_\alpha$  dependence of the  $\alpha$ -cluster probability. If a  $^{14}\text{N}$

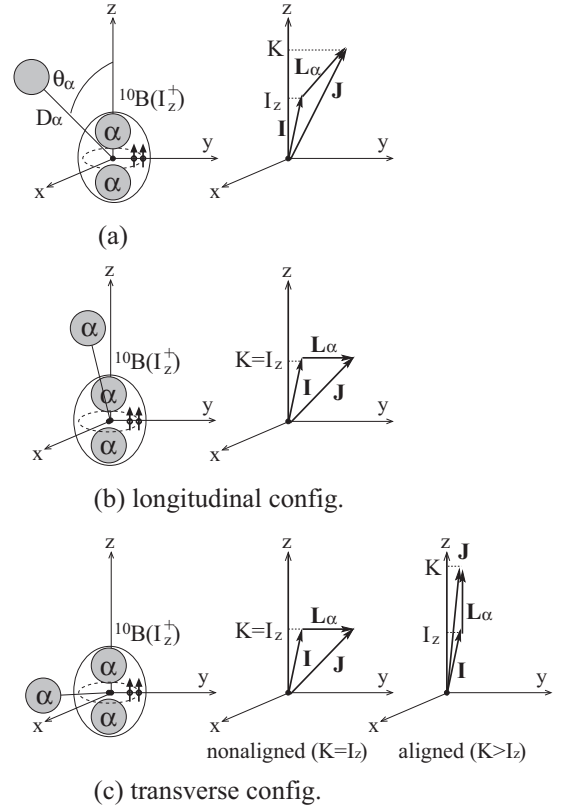


FIG. 2. Schematic figures for  $\Phi_{^{10}\text{B}(I_z^\pi)+\alpha}(D_\alpha, \theta_\alpha)$  in Eq. (8) and those for  $L_\alpha$  orientation in the  $JK$ -projected states. (a) Left: A configuration for  $\Phi_{^{10}\text{B}(I_z^\pi)+\alpha}(D_\alpha, \theta_\alpha)$  in Eq. (8) for the  $\alpha$  cluster at  $(D_\alpha, \theta_\alpha)$  around the  $I_z^\pi$ -projected  $^{10}\text{B}$  cluster. Right: Angular momenta in the  $JK$ -projected state of  $\Phi_{^{10}\text{B}(I_z^\pi)+\alpha}(D_\alpha, \theta_\alpha)$ . (b) Same as panel (a) but for the longitudinal configuration ( $\theta_\alpha \sim 0$ ).  $K$  is restricted to be  $K = I_z$  because of the axial symmetry. (c) Left: Transverse configuration for  $\theta_\alpha \sim \pi/2$ . Middle: Angular momenta in the  $JK$ -projected state of the transverse configuration for the nonaligned ( $K = I_z$ ) case. Right: Angular momenta in the  $JK$ -projected state of the transverse configuration for the aligned ( $K > I_z$ ) case.

state is a weak coupling state dominated by a  $^{10}\text{B}(I^\pi) \otimes L_\alpha$  component, the probability is distributed widely in the entire  $\theta_\alpha$  region without the concentration in a certain  $\theta$  region. In other words, if the probability of a  $^{14}\text{N}$  state is not distributed widely, but concentrates on a certain  $\theta$  region, this means that the state is a strong-coupling state containing an enhanced component of the corresponding geometric configuration rather than a weak-coupling state.

**2.  $^{10}\text{B}(I^\pi) \otimes L_\alpha$  components based on the weak-coupling picture**

I evaluate  $^{10}\text{B}(3^+) \otimes L_\alpha$  and  $^{10}\text{B}(1^+) \otimes L_\alpha$  components by the  $L_\alpha$  projection. I consider the  $L_\alpha L_{\alpha z}$ -projected  $^{10}\text{B}(I_z^\pi) + \alpha$  wave function,

$$|J; ^{10}\text{B}(I_z^\pi); D_\alpha, L_\alpha L_{\alpha z}\rangle = n_0 \sum_{\theta_\alpha} \omega(\theta_\alpha) y_{L_{\alpha z}}^{L_\alpha}(\theta_\alpha) \hat{P}_{MK=I_z+L_{\alpha z}}^{JK} \Phi_{^{10}\text{B}(I_z^\pi)+\alpha}(D_\alpha, \theta_\alpha), \quad (10)$$

with  $X_\alpha - X_B = (D_\alpha \sin \theta_\alpha, 0, D_\alpha \cos \theta_\alpha)$  and  $4X_\alpha + 10X_B = 0$ .  $y_\mu^\lambda(\theta)$  is the  $\theta$ -dependent part of the spherical harmonics  $Y_\mu^\lambda(\theta, \phi)$  and is given as  $y_\mu^\lambda(\theta) = e^{-i\mu\phi} Y_\mu^\lambda(\theta, \phi)$ . The parity  $\pi$  in the projection operator  $\hat{P}_{MK}^{J\pi}$  is the same as that of  $I_z^\pi$  and is positive ( $\pi = +$ ) in the present paper.  $n_0$  is determined from the normalization condition  $\langle J; {}^{10}\text{B}(I_z^\pi); D_\alpha, L_\alpha L_{\alpha z} | J; {}^{10}\text{B}(I_z^\pi); D_\alpha, L_\alpha L_{\alpha z} \rangle = 1$ . In Eq. (10), the  $L_{\alpha z}$  projection is done by the  $K$  projection in the projection operator  $\hat{P}_{MK}^{J\pi}$  with  $K = I_z + L_{\alpha z}$ . The  $L_\alpha$  projection is approximately performed by the summation  $\theta_\alpha = \frac{\pi}{N_\theta} i$  ( $i = 0, \dots, N_\theta$ ) with the weight function  $\omega(\theta_\alpha) = \int_{\min[\theta_\alpha - \pi/2N_\theta, 0]}^{\max[\theta_\alpha + \pi/2N_\theta, \pi]} \sin \theta d\theta$ . I perform only  $L_\alpha = 0$  and  $L_\alpha = 2$  projections because  $L_\alpha \geq 4$  projections are not possible for the present  $N_\theta = 4$  case. I calculate the squared overlap of the  ${}^{14}\text{N}$  wave function with the above wave function,  $|\langle J; {}^{10}\text{B}(I_z^\pi); D_\alpha, L_\alpha L_{\alpha z} | \Psi_{14\text{N}(J_n^\pi)} \rangle|^2$ . Assuming that the  $3_1^+$  and  $1_1^+$  states of the  ${}^{10}\text{B}$  cluster are approximately described by the  $I_z^\pi$ -projected  ${}^{10}\text{B}$  wave functions,  ${}^{10}\text{B}(I_z^\pi = 3^+)$  and  ${}^{10}\text{B}(I_z^\pi = 1^+)$ , respectively, I approximately estimate the  ${}^{10}\text{B}(I_z^\pi) \otimes (L_\alpha = 0, 2)$  components in the  ${}^{14}\text{N}$  wave function  $\Psi_{14\text{N}(J_n^\pi)}$  as

$$P_{10\text{B}(I_z^\pi) \otimes L_\alpha}(D_\alpha) \approx \sum_{L_{\alpha z}} |\langle JK | I I_z L_\alpha L_{\alpha z} \rangle \langle J; {}^{10}\text{B}(I_z^\pi); D_\alpha, L_\alpha L_{\alpha z} | \Psi_{14\text{N}(J_n^\pi)} \rangle|^2, \quad (11)$$

with  $I_z = I$  and  $K = I_z + L_{\alpha z}$ , where  $\langle JK | I I_z L_\alpha L_{\alpha z} \rangle$  is the Clebsch-Gordan coefficient.

If a  ${}^{14}\text{N}$  state is a weak-coupling state dominated by a  ${}^{10}\text{B}(I_z^\pi) \otimes L_\alpha$  component, the probability is concentrated on the corresponding  $L_\alpha$  state. If a  ${}^{14}\text{N}$  state is a strong-coupling state, the probability is fragmented into various  $L_\alpha$  components reflecting the large  $L_\alpha$  mixing.

### III. RESULTS

I adopt the two-body effective nuclear interactions used in Ref. [58] that are adjusted to describe low-lying energy levels of  ${}^{10}\text{B}$ . Namely, I use the Volkov central force [60] with the Bartlett, Heisenberg, and Majorana parameters  $b = h = 0.006$  and  $m = 0.60$ , the G3RS spin-orbit force [61] with the strength  $u_I = -u_{II} = 1300$  MeV, and the Coulomb force approximated by 7-range Gaussian. Using these interactions, energies of  ${}^{10}\text{B}$  are obtained to be  $-53.3$  MeV for the ground state ( $3^+$ ) and  $-52.2$  MeV for the first excited state ( $1^+$ ) with the  $2\alpha + pn$ -cluster model by superposing  $\sum_{I_z, d} \hat{P}_{MI_z}^{I\pi} \Phi_{10\text{B}}(\mathbf{X}_B = 0; d, \phi = 0)$  with  $d = 1$  and 2 (fm). Though the calculation underestimates the experimental binding energy (64.75 MeV), it reproduces the spin-parity of the ground state [ ${}^{10}\text{B}(3_{\text{g.s.}}^+)$ ], and also the calculated excitation energy  $E_x = 0.9$  MeV of the  $1^+$  state reasonably agrees with the experimental value  $E_x = 0.72$  MeV for  ${}^{10}\text{B}(1_1^+)$ . Properties of  ${}^{10}\text{B}(3_{\text{g.s.}}^+)$  such as the magnetic moment ( $\mu$ ), the electric quadrupole moment ( $Q$ ), and the rms radius of proton distribution ( $r_p$ ) are calculated to be  $\mu = 1.83$  ( $\mu_N$ ),  $Q = 8.1$  ( $e \text{ fm}^2$ ), and  $r_p = 2.35$  (fm), which are in reasonable agreement with the experimental data,

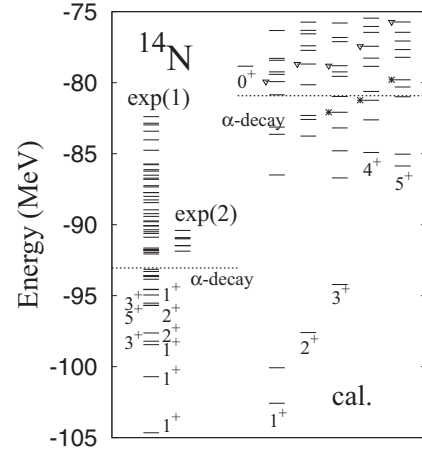


FIG. 3. Positive-parity energy levels of  ${}^{14}\text{N}$  obtained by the  ${}^{10}\text{B} + \alpha$ -cluster model compared with experimental levels taken from Ref. [62].  ${}^{10}\text{B} + \alpha$ -cluster states in the  $K^\pi = 3^+$  band and those in the  $K^\pi = 1^+$  band are labeled by asterisks and down-triangle symbols, respectively. The dotted lines indicate the  $\alpha$ -decay threshold.

$\mu = 1.80$  ( $\mu_N$ ),  $Q = 8.472(56)$  ( $e \text{ fm}^2$ ), and  $r_p = 2.25(5)$  (fm) reduced from the charge radius.

Using the  ${}^{10}\text{B} + \alpha$ -cluster wave function in Eq. (7), I calculate positive-parity states of  ${}^{14}\text{N}$ . Properties of the ground state  ${}^{14}\text{N}(1_{\text{g.s.}}^+)$  are reasonably reproduced by the present calculation. Namely, the calculated values, the binding energy B.E. = 102.6 MeV,  $\mu = 0.36$  ( $\mu_N$ ),  $Q = 2.4$  ( $e \text{ fm}^2$ ), and  $r_p = 2.38$  (fm) of  ${}^{14}\text{N}(1_{\text{g.s.}}^+)$ , reasonably agree with the experimental data [B.E. = 104.66 MeV,  $\mu = 0.4038$  ( $\mu_N$ ),  $Q = 1.93(8)$  ( $e \text{ fm}^2$ ),  $r_p = 2.39(1)$  (fm)]. The calculated energy spectra are shown in Fig. 3. The  $\alpha$ -decay threshold is much higher in the present calculation than the experimental threshold. In other words, the ground and some low-lying states of  ${}^{14}\text{N}$  show too deep binding from the  $\alpha$ -decay threshold compared with the experimental data. The significant overestimation of the  $\alpha$ -decay threshold is a general problem in microscopic calculations with density-independent two-body effective interactions as found for  ${}^{14}\text{C}$  and O isotopes [6, 31, 33]. One of the origins of this problem is a difficulty in reproducing systematics of binding energies in a wide mass-number region with such effective interactions. In the present calculation, only the  ${}^{14}\text{N}$  states that can be approximately described by the model space of the present  $(2\alpha) + (pn) + \alpha$ -cluster model are obtained but states such as other spin configuration states and single-particle excitations may be missing.

In this paper, I mainly investigate  ${}^{10}\text{B} + \alpha$ -cluster states near the  $\alpha$ -decay threshold and discuss their features. In the calculated energy levels near the threshold, I obtain several excited states having significant component of a spatially developed  $\alpha$  cluster around the  ${}^{10}\text{B}$  cluster. From remarkable  $E2$  transitions, I assign the  ${}^{10}\text{B} + \alpha$ -cluster states to a  $K^\pi = 3^+$  band of  $J^\pi = 3^+, 4^+,$  and  $5^+$  states and a  $K^\pi = 1^+$  band of  $J^\pi = 1^+, 2^+, 3^+, 4^+,$  and  $5^+$  states. The former and the latter bands are shown by asterisks and down-triangle symbols in Fig. 3. The  $K^\pi = 3^+$  band has the significant  ${}^{10}\text{B}(3^+) + \alpha$  component, whereas the  $K^\pi = 1^+$  band contains





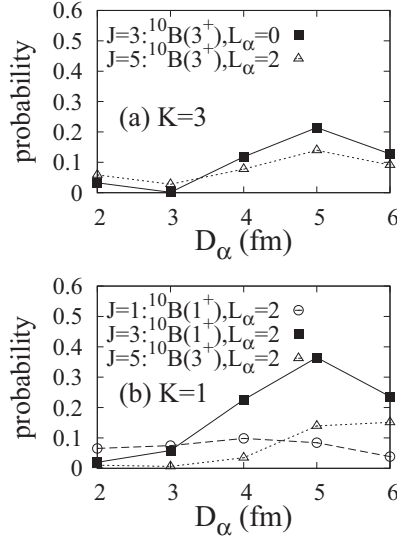


FIG. 6.  $^{10}\text{B}(I^\pi) \otimes L_\alpha$  components [ $P_{^{10}\text{B}(I^\pi) \otimes L_\alpha}(D_\alpha)$  in Eq. (11)] for  $^{10}\text{B} + \alpha$ -cluster states in the  $K^\pi = 3^+$  and  $K^\pi = 1^+$  bands obtained by the full- $D_\alpha$  calculation. The  $D_\alpha$  dependencies of the dominant components for (a)  $J^\pi = 3^+(K^\pi = 3^+)$  and  $5^+(K^\pi = 3^+)$  and for (b)  $J^\pi = 1^+(K^\pi = 1^+)$ ,  $J^\pi = 3^+(K^\pi = 1^+)$ , and  $5^+(K^\pi = 1^+)$  are shown.

The level structures of the  $K^\pi = 3^+$  and  $K^\pi = 1^+$  bands are essentially consistent between the full- $D_\alpha$  and fixed- $D_\alpha$  calculations, though about a 2-MeV global shift is found for the  $K^\pi = 3^+$  band between two calculations.

### B. $\alpha$ -cluster probability and $\alpha$ -decay widths

I show in Fig. 6  $^{10}\text{B}(I^\pi) \otimes L_\alpha$  components [ $P_{^{10}\text{B}(I^\pi) \otimes L_\alpha}(D_\alpha)$  in Eq. (11)] for  $^{10}\text{B} + \alpha$ -cluster states in the  $K^\pi = 3^+$  and  $K^\pi = 1^+$  bands obtained by the full- $D_\alpha$  calculation. The probability for the dominant channel shows the maximum amplitude at  $D_\alpha \sim 5$  fm. In Table I, I show  $P_{^{10}\text{B}(I^\pi) \otimes L_\alpha}(D_\alpha)$  at  $D_\alpha = 5$  fm in  $^{10}\text{B} + \alpha$ -cluster states obtained by the full- $D_\alpha$  and fixed- $D_\alpha$  calculations. In the result of the fixed- $D_\alpha$  calculation,  $K^\pi = 3^+$  band states are dominated by the  $^{10}\text{B}(3^+) \otimes L_\alpha$  component, whereas  $K^\pi = 1^+$  band states contain dominantly the  $^{10}\text{B}(1^+) \otimes L_\alpha$  component. In the result of the full- $D_\alpha$  calculation, the dominant channel of each state in the  $K^\pi = 3^+$  and  $K^\pi = 1^+$  bands is essentially consistent with that in the fixed- $D_\alpha$  calculation, except for the  $1^+(K^\pi = 1^+)$  state, though the absolute amplitude of the dominant component decreases because of radial motion and state mixing. Namely, the  $K^\pi = 3^+$  and  $K^\pi = 1^+$  band states except for the  $1^+(K^\pi = 1^+)$  state contain significant  $^{10}\text{B}(3^+) \otimes L_\alpha$  and  $^{10}\text{B}(1^+) \otimes L_\alpha$  components, respectively, also in the full- $D_\alpha$  calculation. The  $1^+(K^\pi = 1^+)$  state obtained by the full- $D_\alpha$  calculation shows a feature quite different from that obtained by the fixed- $D_\alpha$  calculation, which has almost the pure  $^{10}\text{B}(1^+) \otimes (L_\alpha = 0)$  component showing a weak-coupling feature. That is, the  $1^+(K^\pi = 1^+)$  state in the full- $D_\alpha$  calculation has  $^{10}\text{B}(1^+) \otimes (L_\alpha = 0)$ ,  $^{10}\text{B}(1^+) \otimes (L_\alpha = 2)$ , and  $^{10}\text{B}(3^+) \otimes (L_\alpha = 2)$  components with the same order showing a strong-coupling feature.

TABLE I.  $^{10}\text{B}(I^\pi) \otimes (L_\alpha = 0, 2)$  components,  $P_{^{10}\text{B}(I^\pi) \otimes L_\alpha}(D_\alpha = 5 \text{ fm})$ , of  $^{10}\text{B} + \alpha$ -cluster states in the  $K^\pi = 3^+$  and  $K^\pi = 1^+$  bands obtained by the full- $D_\alpha$  and fixed- $D_\alpha$  calculations.

$J^\pi$	$P_{^{10}\text{B}(3^+) \otimes L_\alpha}$		$P_{^{10}\text{B}(1^+) \otimes L_\alpha}$	
	$L_\alpha = 0$	$L_\alpha = 2$	$L_\alpha = 0$	$L_\alpha = 2$
Full- $D_\alpha$ cal.				
$3^+(K^\pi = 3^+)$	0.21	0.10		0.04
$4^+(K^\pi = 3^+)$		0.23		
$5^+(K^\pi = 3^+)$		0.14		
$1^+(K^\pi = 1^+)$		0.03	0.05	0.09
$2^+(K^\pi = 1^+)$		0.02		0.25
$3^+(K^\pi = 1^+)$	0.00	0.02		0.37
$4^+(K^\pi = 1^+)$		0.01		
$5^+(K^\pi = 1^+)$		0.14		
Fixed- $D_\alpha$ cal.				
$3^+(K^\pi = 3^+)$	0.57	0.25		0.01
$4^+(K^\pi = 3^+)$		0.73		
$5^+(K^\pi = 3^+)$		0.75		
$1^+(K^\pi = 1^+)$		0.02	0.89	0.05
$2^+(K^\pi = 1^+)$		0.01		0.78
$3^+(K^\pi = 1^+)$	0.10	0.13		0.74
$4^+(K^\pi = 1^+)$		0.00		

Figure 7 shows  $L_\alpha$  components ( $P_{^{10}\text{B}(I^\pi) \otimes L_\alpha}$ ) at  $D_\alpha = 5$  fm of  $J^\pi$  states in the  $^{14}\text{N}$  spectra obtained by the full- $D_\alpha$  calculation. The  $^{10}\text{B}(3^+) \otimes (L_\alpha = 0)$  and  $^{10}\text{B}(3^+) \otimes (L_\alpha = 2)$  components concentrate at the  $3^+(K^\pi = 3^+)$  and  $4^+(K^\pi = 3^+)$  states, respectively, though the components are fragmented

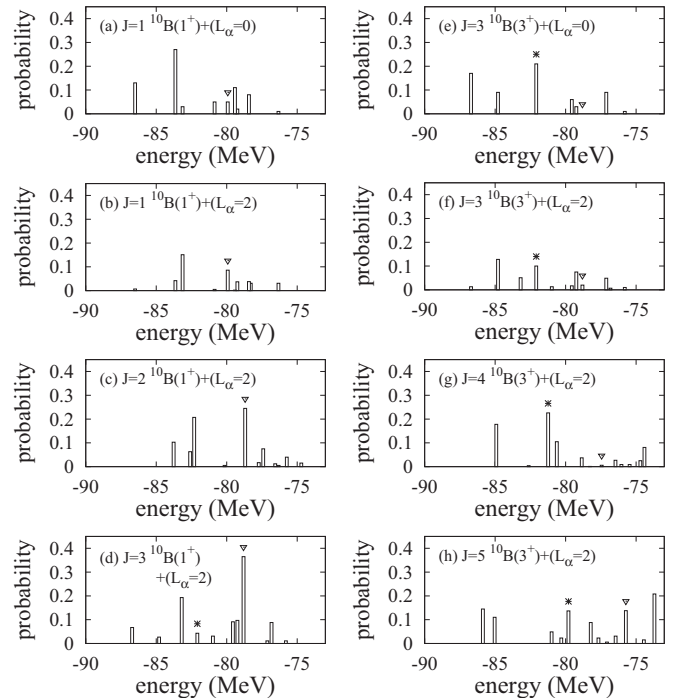


FIG. 7.  $^{10}\text{B}(I^\pi) \otimes (L_\alpha = 0, 2)$  components,  $P_{^{10}\text{B}(I^\pi) \otimes L_\alpha}(D_\alpha = 5 \text{ fm})$ , in positive-parity states of  $^{14}\text{N}$  obtained by the  $^{10}\text{B} + \alpha$  cluster model. Asterisks and down-triangle symbols show  $^{10}\text{B} + \alpha$ -cluster states in the  $K^\pi = 3^+$  and  $K^\pi = 1^+$  bands, respectively.

into other states. The  $5^+(K^\pi = 3^+)$  state shows rather strong state mixing. The  $^{10}\text{B}(1^+) \otimes (L_\alpha = 2)$  component concentrates at the  $2^+(K^\pi = 1^+)$  and  $3^+(K^\pi = 1^+)$  states, whereas, the  $^{10}\text{B}(1^+) \otimes (L_\alpha = 0)$  component feeds lower  $1^+$  states of  $^{14}\text{N}$ .

In the experiment of  $^{10}\text{B}(\alpha, \alpha)^{10}\text{B}$  reactions [57], the  $3^+$  state at  $E_r = 1.58$  MeV ( $E_x = 13.19$  MeV) with the width  $\Gamma = 0.065$  MeV is strongly populated. In the analysis of Ref. [57], this state is described well by the dominant (almost 100%)  $S$ -wave  $\alpha$ -decay indicating the significant  $^{10}\text{B}(3^+) \otimes (L_\alpha = 0)$  component of the  $3^+$  state. The  $1^+$  state at  $E_r = 2.11$  MeV ( $E_x = 13.72$  MeV) is weakly populated in  $^{10}\text{B}(\alpha, \alpha)^{10}\text{B}$  reactions, whereas its  $\alpha$  decay into the first excited state of  $^{10}\text{B}(1^+)$  was observed in  $^{10}\text{B}(\alpha, \alpha')^{10}\text{B}$  reactions [63]. These experiments suggest that the  $1^+$  state would contain  $^{10}\text{B}(1^+) \otimes (L_\alpha = 0)$  and  $^{10}\text{B}(3^+) \otimes (L_\alpha = 2)$  components.

From the experimental  $\alpha$ -decay properties, I tentatively assign the theoretical  $3^+(K^\pi = 3^+)$  and  $1^+(K^\pi = 1^+)$  states having  $^{10}\text{B} + \alpha$ -cluster structures to the experimental  $3^+$  ( $E_r^{\text{exp}} = 1.58$  MeV) and  $1^+$  ( $E_r^{\text{exp}} = 2.11$  MeV) states, though the bandhead energies  $E_r(3^+; K^\pi = 3^+) = -1.2$  MeV and  $E_r(1^+; K^\pi = 1^+) = 1.0$  MeV obtained by the full- $D_\alpha$  calculation do not necessarily agree with the experimental energies (see Fig. 5). I estimate partial  $\alpha$ -decay widths for  $^{10}\text{B}(I^\pi) \otimes L_\alpha$  channels from  $P_{^{10}\text{B}(I^\pi) \otimes L_\alpha}(D_\alpha = a)$  ( $a$  is the channel radius) as follows. Using the approximate evaluation of the reduced width amplitude proposed in Ref. [64], the reduced width  $\gamma_\alpha^2(a)$  is calculated as

$$\gamma_\alpha^2(a) = \frac{\hbar^2}{2\mu a} \left( \frac{\nu}{2\pi} \frac{A_1 A_2}{A_1 + A_2} \right)^{1/2} P_{^{10}\text{B}(I^\pi) \otimes L_\alpha}(D_\alpha = a), \quad (13)$$

and the partial  $\alpha$ -decay width  $\Gamma_{^{10}\text{B}(I^\pi) + \alpha}$  for  $L_\alpha = l$  is calculated as

$$\Gamma_{^{10}\text{B}(I^\pi) + \alpha} = 2P_l(a)\gamma_\alpha^2(a), \quad (14)$$

$$P_l(a) = \frac{ka}{F_l^2(ka) + G_l^2(ka)}, \quad (15)$$

where  $k = \sqrt{2\mu E}/\hbar$  with the reduced mass  $\mu$ , and  $F_l$  and  $G_l$  are the regular and irregular Coulomb functions, respectively. Here I use the momentum  $k$  of the energy  $E = E_r^{\text{(adjust)}}$ , which is phenomenologically adjusted to the experimental energy position because it is difficult to quantitatively predict the energy position in the present calculation. Namely, I adjust the bandhead energies of the  $K^\pi = 3^+$  and  $K^\pi = 1^+$  bands to the experimental energy positions  $E_r^{\text{exp}}(3^+) = 1.58$  MeV and  $E_r^{\text{exp}}(1^+) = 2.11$  MeV by a constant shift for each band as

$$\begin{aligned} E_r^{\text{(adjust)}}(J^+; K^\pi = 3^+) \\ = E_r(J^+; K^\pi = 3^+) - E_r(3^+; K^\pi = 3^+) + E_r^{\text{exp}}(3^+), \end{aligned} \quad (16)$$

$$\begin{aligned} E_r^{\text{(adjust)}}(J^+; K^\pi = 1^+) \\ = E_r(J^+; K^\pi = 1^+) - E_r(1^+; K^\pi = 1^+) + E_r^{\text{exp}}(1^+). \end{aligned} \quad (17)$$

TABLE II. Partial  $\alpha$ -decay widths of  $^{10}\text{B} + \alpha$ -cluster states in the  $K^\pi = 3^+$  and  $K^\pi = 1^+$  bands obtained by the full- $D_\alpha$  calculation. The channel radius is chosen to be  $a = 5$  fm. Energies of the bandhead states of the  $K^\pi = 3^+$  and  $K^\pi = 1^+$  bands are adjusted to the experimental resonance energies of the  $3^+$  state at 1.58 MeV and the  $1^+$  state at 2.11 MeV. The sum  $[\Gamma_{^{10}\text{B} + \alpha}(L_\alpha \leq 2)]$  of the partial widths of the decay channels  $^{10}\text{B}(3^+) \otimes (L_\alpha \leq 2)$  and  $^{10}\text{B}(1^+) \otimes (L_\alpha \leq 2)$  is also shown. The unit is MeV.

$J^\pi$	$E_r^{\text{(adjust)}}$	$\Gamma_{^{10}\text{B}(3^+) + \alpha}$		$\Gamma_{^{10}\text{B}(1^+) + \alpha}$		$\Gamma_{^{10}\text{B}(3^+) + \alpha}$ ( $L_\alpha \leq 2$ )
		$L_\alpha = 0$	$L_\alpha = 2$	$L_\alpha = 0$	$L_\alpha = 2$	
$3^+(K^\pi = 3^+)$	1.58	0.04	0.00		0.00	0.05
$4^+(K^\pi = 3^+)$	2.43		0.06			0.06
$5^+(K^\pi = 3^+)$	3.87		0.16			0.16
$1^+(K^\pi = 1^+)$	2.11		0.00	0.01	0.00	0.01
$2^+(K^\pi = 1^+)$	3.35		0.02		0.09	0.11
$3^+(K^\pi = 1^+)$	3.23	0.00	0.01		0.12	0.13
$4^+(K^\pi = 1^+)$	4.60		0.01			0.01
$5^+(K^\pi = 1^+)$	6.31		0.36			0.36

Calculated partial  $\alpha$ -decay widths obtained by the full- $D_\alpha$  calculation are shown in Table II. I calculate widths for  $L_\alpha = 0$  and  $L_\alpha = 2$  channels for the channel radius  $a = 5$  fm. The  $\alpha$ -decay width of the  $3^+(K^\pi = 3^+)$  state is  $\Gamma_\alpha = 0.05$  MeV with the dominant  $^{10}\text{B}(3^+) \otimes (L_\alpha = 0)$  decay, which is quantitatively consistent with the experimental observation [ $\Gamma_\alpha \sim \Gamma = 0.065(10)$  MeV] [57]. For the  $1^+(K^\pi = 1^+)$  state, I obtain a small  $\alpha$ -decay width  $\Gamma_\alpha = 0.01$  MeV with the dominant  $^{10}\text{B}(1^+) \otimes (L_\alpha = 0)$  decay. This result seems consistent with the weak population in the  $\alpha$  elastic scattering [57] and the fact that the  $1^+$  state was observed in the  $^{10}\text{B}(\alpha, \alpha')^{10}\text{B}$  reaction [63]. However, experimental information of partial  $\alpha$ -decay widths is not enough to confirm the present assignment of the  $1^+(K^\pi = 1^+)$  state. The calculated  $\alpha$ -decay width is much smaller than the experimental total width,  $\Gamma = 0.16(2)$  MeV, of the  $1^+$  state at 2.11 MeV. I should comment that, because the  $^{10}\text{B}(1^+) \otimes (L_\alpha = 0)$  component is fragmented into neighboring states as shown in Fig. 7, an effectively large width could be observed for the  $1^+(K^\pi = 1^+)$  state.

### C. Angular motion of the $\alpha$ cluster around the deformed $^{10}\text{B}$ cluster

I here discuss angular motion of the  $\alpha$  cluster around the deformed  $^{10}\text{B}$  cluster by analyzing the  $\theta_\alpha$  dependence of  $\alpha$ -cluster probabilities. Discussions in this section are based on the strong-coupling picture, which is somehow different from the previous discussion based on the  $L_\alpha$  decomposition in the weak-coupling picture. I show energies of  $\Phi_{^{10}\text{B}(I_z^\pi) + \alpha}(D_\alpha, \theta_\alpha)$ , in which the  $\alpha$  cluster is localized at  $(D_\alpha, \theta_\alpha)$  around the  $I_z^\pi$ -projected  $^{10}\text{B}$  cluster. In Fig. 8, intrinsic energies before parity and angular momentum projections of  $\Phi_{^{10}\text{B}(I_z^\pi) + \alpha}(D_\alpha, \theta_\alpha)$  for  $I_z^\pi = 3^+$  and  $1^+$  are plotted on the  $(x, z) = (D_\alpha \sin \theta_\alpha, D_\alpha \cos \theta_\alpha)$  plane. The energy curves for  $D_\alpha = 5$  fm are also shown as functions of  $\theta_\alpha$ . In the  $D_\alpha \geq 5$  fm region, the contour of the energy surface on the  $(x, z)$  plane is deformed in the longitudinal ( $\theta_\alpha = 0$ ) direction because of



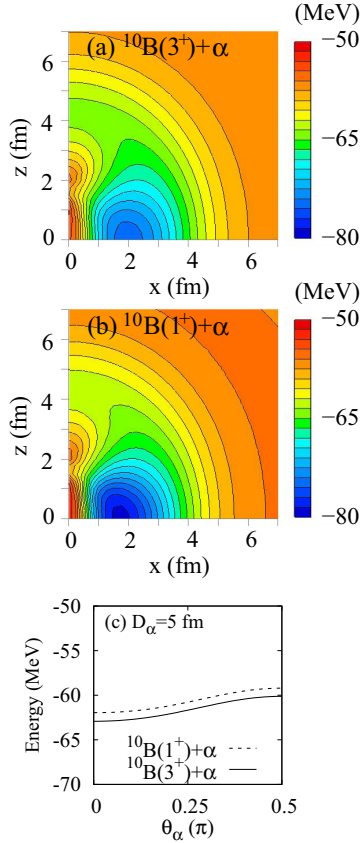


FIG. 8. (Color online) Intrinsic energies of  $^{10}\text{B}(I_z^\pi = 3^+) + \alpha$  and  $^{10}\text{B}(I_z^\pi = 1^+) + \alpha$  before the parity and angular-momentum projections. Energies for (a)  $^{10}\text{B}(I_z^\pi = 3^+) + \alpha$  and (b)  $^{10}\text{B}(I_z^\pi = 1^+) + \alpha$  plotted on  $(x, z) = (D_\alpha \sin \theta_\alpha, D_\alpha \cos \theta_\alpha)$ , and (c) those at  $D_\alpha = 5$  fm plotted as functions of  $\theta_\alpha$ .

the prolate deformation of the  $^{10}\text{B}$  cluster, meaning that the  $\alpha$  cluster at the fixed distance  $D_\alpha = 5$  fm feels an attraction in the longitudinal direction. In other words, in the intrinsic system, the  $\alpha$  cluster at  $D_\alpha = 5$  fm energetically favors the longitudinal direction to form the linear  $3\alpha$  configuration rather than the transverse direction to form the triangle  $3\alpha$  configuration. In the  $D_\alpha \leq 3$  fm region, the  $\alpha$  cluster feels an effective repulsion in the longitudinal direction because of the Pauli blocking from the  $^{10}\text{B}$  cluster, whereas it feels an attraction in the transverse ( $\theta_\alpha = \pi/2$ ) direction.

In contrast to the intrinsic energy behavior, the  $\theta_\alpha$  dependence of the  $J^\pi$  projected energy is not trivial because the energy is affected by not only potential energy but also by the kinetic energy of angular motion, i.e., rotational energy. Figure 9 shows energies of  $JK$ -projected states  $[\hat{P}_{MK}^{J^\pi} \Phi_{^{10}\text{B}(I_z^\pi)+\alpha}(D_\alpha, \theta_\alpha)]$  of  $\Phi_{^{10}\text{B}(I_z^\pi)+\alpha}(D_\alpha, \theta_\alpha)$  at  $D_\alpha = 5$  fm for  $K = I_z$ , which corresponds to the  $L_{\alpha z} = 0$  projection. In high- $J$  states, the longitudinal direction ( $|\theta_\alpha| \lesssim \pi/8$ ) is energetically favored more than the transverse direction ( $|\theta_\alpha - \pi/2| \lesssim \pi/8$ ) because the longitudinal configuration has a moment of inertia (m.o.i.) larger than that of the transverse configuration for the  $L_{\alpha z} = 0$  projection. However, in the lowest-spin state ( $JK = 11$ ), the energy almost degenerates

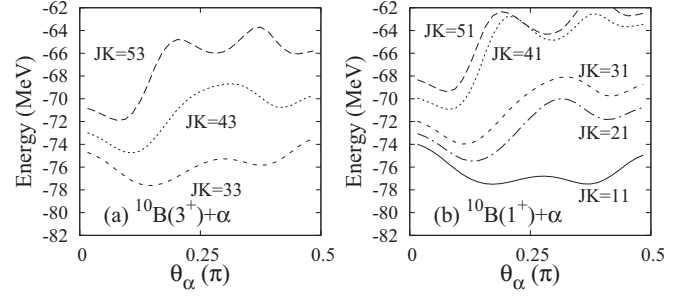


FIG. 9. Energies of the  $JK$ -projected  $\Phi_{^{10}\text{B}(I_z^\pi)+\alpha}$  wave function  $\hat{P}_{MK}^{J^\pi} \Phi_{^{10}\text{B}(I_z^\pi)+\alpha}(D_\alpha, \theta_\alpha)$  with  $K = I_z$  for (a)  $^{10}\text{B}(I_z^\pi = 3^+) + \alpha$  and (b)  $^{10}\text{B}(I_z^\pi = 1^+) + \alpha$ . Energies for  $D_\alpha = 5$  fm are plotted as functions of  $\theta_\alpha$ .

in a wide region of  $\theta_\alpha$  because the kinetic energy for the transverse configuration is smaller than that for the longitudinal configuration because of the phase-space factor  $\sin \theta_\alpha$  in the  $L_{\alpha z} = 0$  projection. This energy degeneracy results in the  $L_\alpha = 0$  ( $S$ -wave) dominance in the  $1^+(K^\pi = 1^+)$  state obtained by the fixed- $D_\alpha$  calculation.

Figures 10 and 11 show energies of  $JK$ -projected states at  $D_\alpha = 5$  fm for  $K \neq I_z$ . Note that the  $K \neq I_z$  projection corresponds to the  $L_{\alpha z} \neq 0$  projection, and  $K > I_z$  means the  $L_\alpha$  alignment to the  $z$  direction [see Fig. 1(c)]. For instance, the  $L_\alpha$ -aligned state for  $L_\alpha = 2$  ( $D$ -wave) is the  $K = I_z + 2$  state. As shown in Figs. 10(a)–10(c) and 11(a)–10(d),  $L_\alpha$ -aligned states energetically favor the transverse configuration because its m.o.i. is larger than that of the longitudinal configuration in the  $L_{\alpha z} = 2$  projection.

Figures 10 and 11 also show the  $\alpha$ -cluster probability  $P(JK, ^{10}\text{B}(I_z^\pi); D_\alpha, \theta_\alpha)$  at  $D_\alpha = 5$  fm in the  $^{10}\text{B} + \alpha$ -cluster states obtained by the fixed- $D_\alpha$  and full- $D_\alpha$  calculations. Let me first discuss the result obtained by the fixed- $D_\alpha$  calculation [Figs. 10(d)–10(f) and 11(e)–10(h)]. In the  $K^\pi = 3^+$  band states [Figs. 10(d)–10(f)], the  $J^\pi = 3^+$  state contains dominantly the longitudinal configuration ( $|\theta_\alpha| \lesssim \pi/8$ ) rather than the transverse configuration ( $|\theta_\alpha - \pi/2| \lesssim \pi/8$ ) as expected from the  $JK$ -projected energy curve for  $K = I_z$ . As the spin ( $J$ ) goes up to  $J = 5$ , the  $L_\alpha$ -aligned component ( $K = 5$ ) of the transverse configuration becomes large corresponding to the alignment of the orbital angular momentum  $L_\alpha$  of the  $\alpha$  cluster to  $I_z = 3$  [the spin of ( $pn$ ) cluster in the  $^{10}\text{B}$  cluster]. In the  $K^\pi = 1^+$  band states [Figs. 11(e)–11(h)], the  $J^\pi = 1^+$  state shows the  $\alpha$ -cluster probability distributed widely in the  $0 \leq \theta_\alpha \leq \pi/2$  region indicating the dominant  $L_\alpha = 0$  ( $S$ -wave) component. As  $J$  increases, the longitudinal component becomes dominant compared with the transverse component. The alignment of  $L_\alpha$  (the orbital angular momentum of the  $\alpha$  cluster) and  $I_z$  is not so remarkable for  $^{10}\text{B}(I_z^\pi = 1^+)$  differently from  $^{10}\text{B}(I_z^\pi = 3^+)$ .

Next, I look into the  $\alpha$ -cluster probability in the full- $D_\alpha$  calculation shown in Figs. 10(g)–10(i) and 11(i)–11(l). The full- $D_\alpha$  calculation shows features of the angular distribution similar to those of the fixed- $D_\alpha$  calculation, except for the  $J^\pi = 1^+$  ( $K^\pi = 1^+$ ) state, though the absolute values of the probability decrease by about a factor of 2. In other words, the  $^{10}\text{B} + \alpha$ -cluster states obtained by the fixed- $D_\alpha$

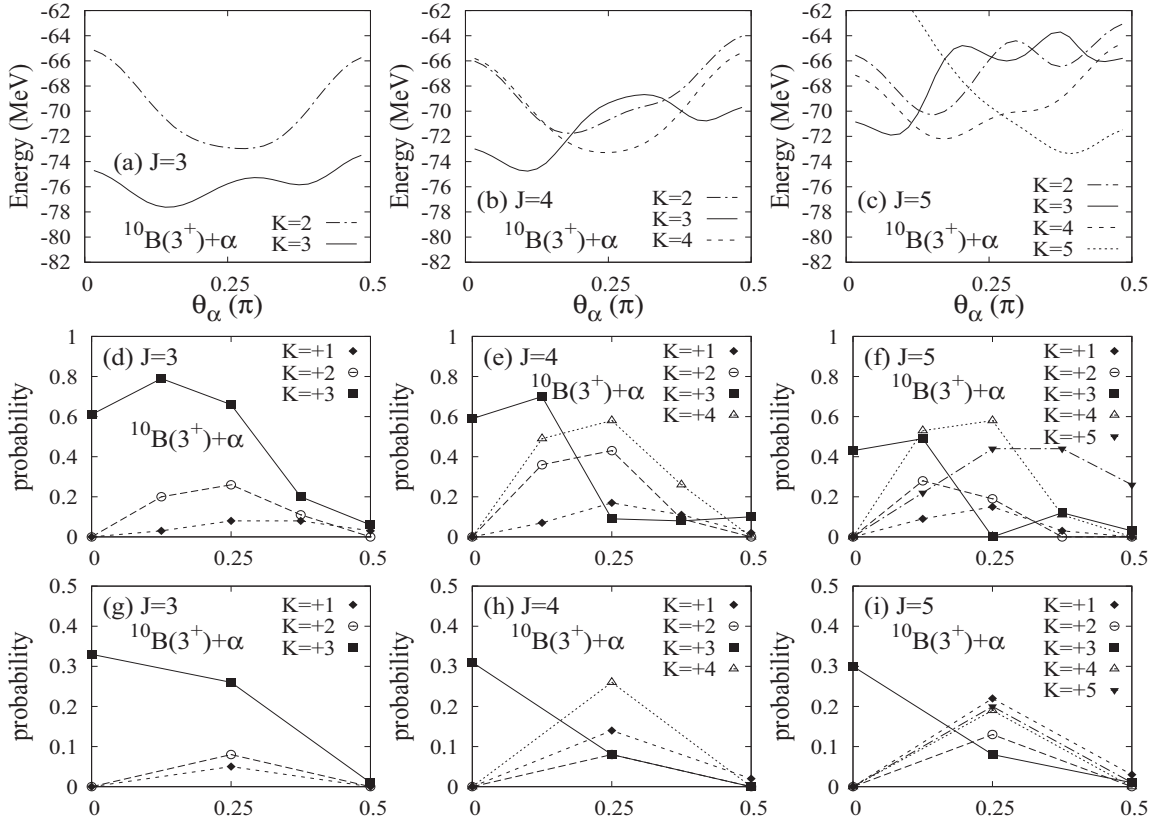


FIG. 10. (a)–(c) Energies of the  $JK$ -projected  $\Phi_{^{10}\text{B}(I_z^\pi)+\alpha}$  wave function  $\hat{P}_{MK}^{J\pi} \Phi_{^{10}\text{B}(I_z^\pi)+\alpha}(D_\alpha, \theta_\alpha)$  for  $^{10}\text{B}(I_z^\pi = 3^+)$ . (d)–(f)  $\alpha$ -cluster probability  $P(JK; ^{10}\text{B}(I_z^\pi); D_\alpha, \theta_\alpha)$  for  $I_z^\pi = 3^+$  at  $D_\alpha = 5$  fm in the  $^{10}\text{B} + \alpha$ -cluster states in the  $K^\pi = 3^+$  band obtained by the fixed- $D_\alpha$  calculation, and (g)–(i) that obtained by the full- $D_\alpha$  calculation.

calculation retain their features in the full- $D_\alpha$  calculation despite the radial motion and state mixing. Compared with the fixed- $D_\alpha$  calculation in more detail, it is found that transverse components tend to be relatively more suppressed than longitudinal components in the full- $D_\alpha$  calculation. In particular in the  $J^\pi = 1^+$  ( $K^\pi = 1^+$ ) state obtained by the full- $D_\alpha$  calculation, the transverse component is significantly suppressed differently from the fixed- $D_\alpha$  calculation. Note that the  $1^+$  ( $K^\pi = 1^+$ ) state obtained by the fixed- $D_\alpha$  calculation contains 90% of the  $^{10}\text{B}(1^+) \otimes (L_\alpha = 0)$  component, in which the  $\alpha$  cluster is moving in almost an  $S$  wave, as discussed previously. Comparing Fig. 11(i) with Fig. 11(e), it is found that the  $1^+$  ( $K^\pi = 1^+$ ) state contains the relatively enhanced longitudinal component and the suppressed transverse component as well as the  $3^+$  ( $K^\pi = 3^+$ ) state, though the absolute amplitude itself decreases in the full calculation because of the radial motion.

Here, it should be noted that the angular distribution of the  $\alpha$ -cluster probability contains the  $\theta_\alpha$ -dependent phase-space factor. In the classical picture, the phase-space factor is  $\sin \theta_\alpha$ . In the present model, the  $\alpha$ -cluster wave function is localized around the position  $\mathbf{R}_\alpha = (D_\alpha \sin \theta_\alpha, 0, D_\alpha \cos \theta_\alpha)$  with a localized Gaussian form,  $f_{\mathbf{R}_\alpha}(\mathbf{r}_\alpha) = (2\nu/\pi)^{3/4} \exp[-\nu_\alpha(\mathbf{r} - \mathbf{R}_\alpha)^2]$ . When the antisymmetrization effect is omitted, the phase-space factor for the positive-parity and  $L_{\alpha z} = 0$  projected state in the strong-coupling limit is estimated by the squared overlap between the positive-parity  $L_{\alpha z} = 0$

component and the  $S$ -wave component of the localized Gaussian as

$$\begin{aligned} \mathcal{N}_{\text{pf}}(D_\alpha, \theta_\alpha) &= \frac{\int d\Omega' \int_0^{2\pi} d\phi_\alpha | \langle f_{\mathbf{R}'_\alpha} | \hat{P}^+ f_{\mathbf{R}_\alpha} \rangle |^2}{\int d\Omega' \int d\Omega \langle f_{\mathbf{R}'_\alpha} | f_{\mathbf{R}_\alpha} \rangle \int_0^{2\pi} d\phi'_\alpha \int_0^{2\pi} d\phi_\alpha \langle \hat{P}^+ f_{\mathbf{R}'_\alpha} | \hat{P}^+ f_{\mathbf{R}_\alpha} \rangle}, \end{aligned} \quad (18)$$

where  $D_\alpha$ ,  $\theta_\alpha$ , and  $\phi_\alpha$  are the spherical coordinates for  $\mathbf{R}_\alpha$ , and  $D_\alpha = D'_\alpha = D''_\alpha$  and  $\theta_\alpha = \theta''_\alpha$  are chosen. As shown in Fig. 12, the phase-space factor  $\mathcal{N}_{\text{pf}}$  is relatively larger in the  $|\theta_\alpha - \pi/2| \lesssim \pi/4$  region for the transverse configuration than in the  $|\theta_\alpha| \lesssim \pi/4$  region for the longitudinal configuration. In Fig. 12, I show the ratio to  $\mathcal{N}_{\text{pf}}$  of the  $\alpha$ -cluster probability  $\hat{P}_{MK}^{J\pi} \Phi_{^{10}\text{B}(I_z^\pi)+\alpha}(D_\alpha, \theta_\alpha)$  for  $K = 3$  and  $I_z^\pi = 3^+$  at  $D_\alpha = 5$  fm in the  $3^+$  ( $K^\pi = 3^+$ ) state and that for  $K = 1$  and  $I_z^\pi = 1^+$  in the  $1^+$  ( $K^\pi = 1^+$ ) state obtained by the full- $D_\alpha$  calculation. The ratios show that the  $\theta_\alpha = 0$  component is remarkably enhanced, whereas the  $\theta_\alpha = \pi/4$  and  $\pi/2$  components are relatively suppressed, indicating a feature of the elongated chain-like structure of the  $^{10}\text{B} + \alpha$ -cluster bands. What I call the “chain-like configuration” is the structure that has relatively enhanced longitudinal components with suppressed transverse components. It should be pointed out that it is different from the ideal linear configuration of a classical picture but it has some quantum fluctuation in the radial and angular ( $\theta_\alpha$ ) motion.

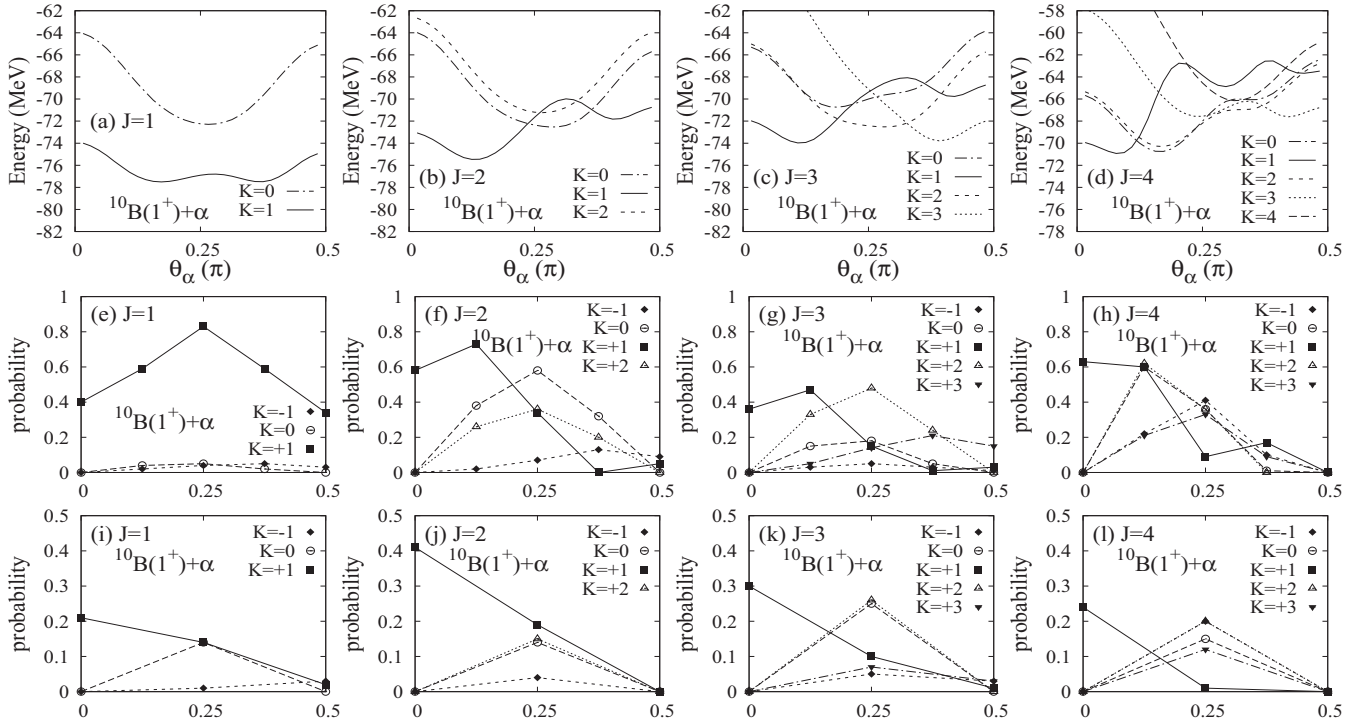


FIG. 11. (a)–(d) Energies of the  $JK$ -projected  $\Phi_{10\text{B}(I_z^\pi)+\alpha}$  wave function  $\hat{P}_{MK}^{J\pi} \Phi_{10\text{B}(I_z^\pi)+\alpha}(D_\alpha, \theta_\alpha)$  for  $^{10}\text{B}(I_z^\pi = 1^+)$ . (e)–(h)  $\alpha$ -cluster probability  $P(JK; ^{10}\text{B}(I_z^\pi); D_\alpha, \theta_\alpha)$  for  $I_z^\pi = 1^+$  at  $D_\alpha = 5$  fm in the  $^{10}\text{B} + \alpha$ -cluster states in the  $K^\pi = 1^+$  band obtained by the fixed- $D_\alpha$  calculation, and (i)–(l) that obtained by the full- $D_\alpha$  calculation.

The origin of the suppression of transverse components in  $^{10}\text{B} + \alpha$ -cluster states in the full- $D_\alpha$  calculation can be described by orthogonality to lower states which contain transverse components with  $D_\alpha < 5$  fm. As shown in Fig. 8 for the energy surface on the  $(D_\alpha, \theta_\alpha)$  plane, an energy pocket exists in the transverse direction ( $\theta_\alpha \sim \pi/2$ ) around  $D_\alpha \sim 2$ , and therefore, transverse components contribute to low-lying  $^{14}\text{N}$  states. Although the low-lying states are compact states containing mainly configurations with small  $D_\alpha$ , transverse

components with  $D_\alpha = 5$  fm somewhat feed the low-lying states. As a result of the feeding of lower states, transverse components in the  $^{10}\text{B} + \alpha$ -cluster states near the threshold are suppressed. Figures 13 and 14 show the  $\alpha$ -cluster probability  $P[JK; ^{10}\text{B}(I_z^\pi); D_\alpha, \theta_\alpha]$  for  $\theta_\alpha = 0$  at  $D_\alpha = 5$  fm and that for  $\theta_\alpha = \pi/4$  and  $\pi/2$  at  $D_\alpha = 4$  fm. (Here  $D_\alpha = 4$  fm is chosen

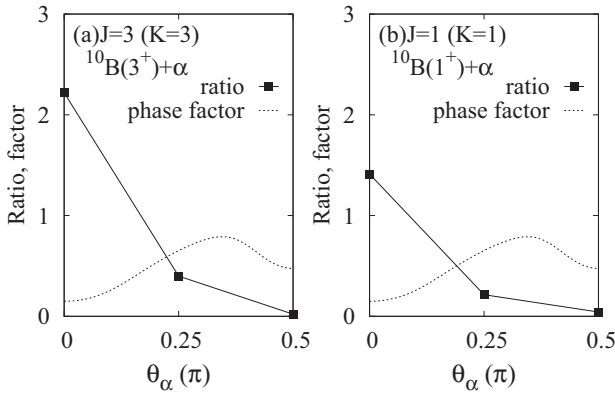


FIG. 12. Ratio of the  $\alpha$ -cluster probability to the phase-space factor  $\mathcal{N}_{\text{pr}}$ . The ratio of the probability  $\hat{P}_{MK}^{J\pi} \Phi_{10\text{B}(I_z^\pi)+\alpha}(D_\alpha, \theta_\alpha)$  for  $K = 3$  and  $I_z^\pi = 3^+$  at  $D_\alpha = 5$  fm in the  $3^+$  ( $K^\pi = 3^+$ ) state and that for  $K = 1$  and  $I_z^\pi = 1^+$  in the  $1^+$  ( $K^\pi = 1^+$ ) state obtained by the full- $D_\alpha$  calculation are shown. The phase-space factor  $\mathcal{N}_{\text{pr}}$  for  $D_\alpha = 5$  fm is also shown.

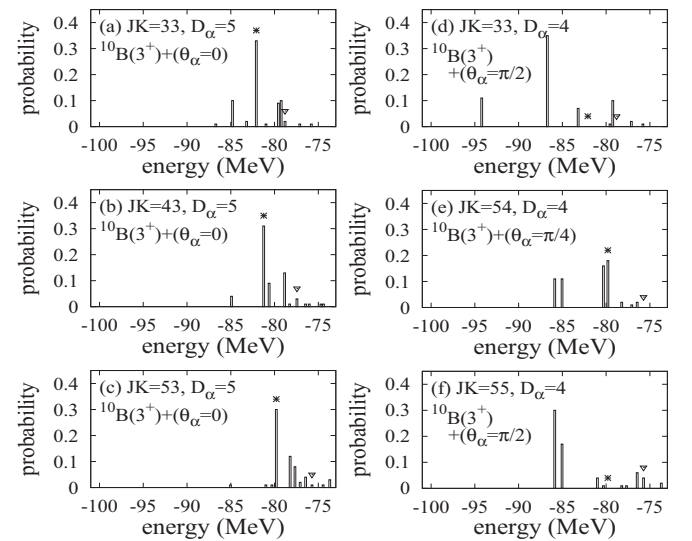


FIG. 13.  $\alpha$ -cluster probability  $P[JK; ^{10}\text{B}(I_z^\pi); D_\alpha, \theta_\alpha]$  for  $I_z^\pi = 3^+$ .  $D_\alpha$  is taken to be  $D_\alpha = 5$  fm for  $\theta_\alpha = 0$  and  $D_\alpha = 4$  fm for  $\theta_\alpha = \pi/4$  and  $\pi/2$ . Asterisks and down-triangle symbols show  $^{10}\text{B} + \alpha$ -cluster states in the  $K^\pi = 3^+$  and  $K^\pi = 1^+$  bands, respectively.

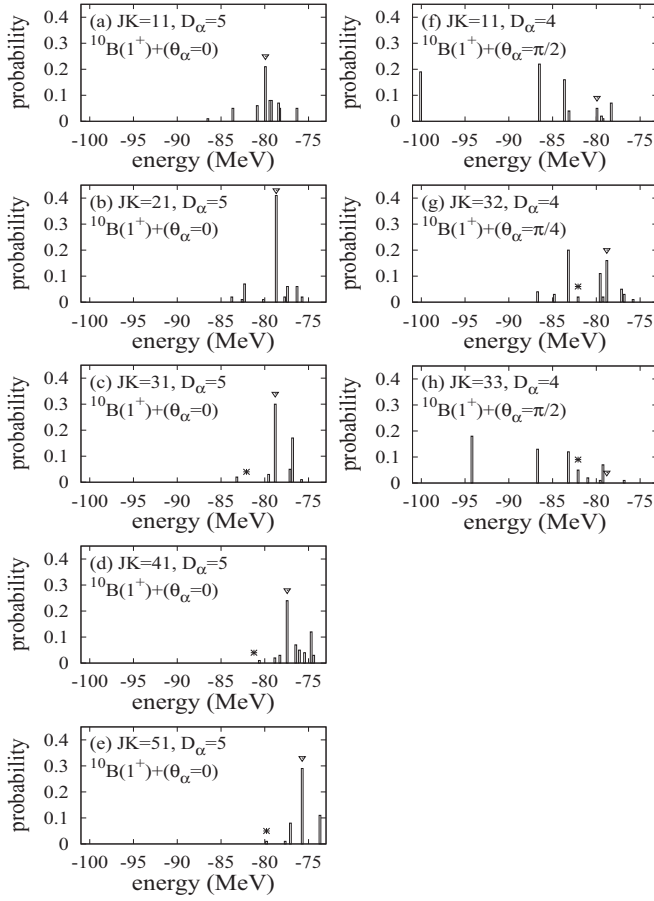


FIG. 14.  $\alpha$ -cluster probability  $P[JK; ^{10}\text{B}(I_z^\pi); D_\alpha, \theta_\alpha]$  for  $I_z^\pi = 1^+$ .  $D_\alpha$  is taken to be  $D_\alpha = 5$  fm for  $\theta_\alpha = 0$  and  $D_\alpha = 4$  fm for  $\theta_\alpha = \pi/4$  and  $\pi/2$ . Asterisks and down-triangle symbols show  $^{10}\text{B} + \alpha$ -cluster states in the  $K^\pi = 3^+$  and  $K^\pi = 1^+$  bands, respectively.

for  $\theta_\alpha = \pi/4$  and  $\pi/2$  just to show the feeding low-lying states of the transverse components at small  $D_\alpha$ , but the probability at  $D_\alpha = 5$  fm is qualitatively consistent with  $D_\alpha = 4$  fm except for the scaling factor.) As seen in Figs. 13(a)–13(c) for  $^{10}\text{B}(I_z^\pi = 3^+)$ , the longitudinal ( $\theta_\alpha = 0$ ) component of  $^{10}\text{B}(I_z^\pi = 3^+) + \alpha$  shows the largest amplitude at the  $K^\pi = 3^+$  band states (labeled by asterisks) and some fragmentation into neighboring states. Similarly, the longitudinal component of  $^{10}\text{B}(I_z^\pi = 1^+) + \alpha$  concentrates on the  $K^\pi = 1^+$  band states [see Figs. 14(a)–14(e)]. On the other hand, transverse

components feed states lower than the  $^{10}\text{B} + \alpha$ -cluster states as seen in Figs. 13(d) and 13(f) and Figs. 14(f) and 14(g). Consequently the  $\alpha$  cluster in  $^{10}\text{B} + \alpha$ -cluster states near the threshold tends to avoid transverse configurations so as to satisfy orthogonality to lower states. This mechanism is consistent with the discussion of Ref. [31] for linear-chain  $3\alpha$  states in  $^{14}\text{C}$ .

## V. SUMMARY

I calculated positive-parity states of  $^{14}\text{N}$  with the  $^{10}\text{B} + \alpha$ -cluster model and investigated  $^{10}\text{B} + \alpha$ -cluster states. Near the  $\alpha$ -decay threshold energy, I obtained the  $K^\pi = 3^+$  and  $K^\pi = 1^+$  rotational bands having the developed  $\alpha$  cluster with the  $^{10}\text{B}(3^+)$  and  $^{10}\text{B}(1^+)$  cores, respectively. I assigned the  $3^+(K^\pi = 3^+)$  state in the present result to the experimental  $3^+$  at  $E_r = 1.58$  MeV observed in  $\alpha$  scattering reactions by  $^{10}\text{B}$  and showed that the calculated  $\alpha$ -decay width agrees with the experimental width.

I analyzed the component of the longitudinal configuration having an  $\alpha$  cluster in the longitudinal direction of the deformed  $^{10}\text{B}$  cluster, which corresponds to a linear-chain  $3\alpha$  structure with valence nucleons. In the spectra of  $^{14}\text{N}$ , the linear-chain component concentrates at the  $^{10}\text{B} + \alpha$ -cluster states in the  $K^\pi = 3^+$  and  $K^\pi = 1^+$  bands. However, the  $^{10}\text{B} + \alpha$ -cluster states are different from the ideal linear configuration of a classical picture but they show significant quantum fluctuation in the angular ( $\theta_\alpha$ ) motion and are regarded as the chain-like configuration that has relatively enhanced longitudinal components and suppressed transverse components. The orthogonality to low-lying states plays an essential role in the suppression of the transverse component.

The present model with the effective interaction cannot quantitatively reproduce the  $\alpha$ -decay threshold energy and the low-energy spectra of  $^{14}\text{N}$ . The influence of the low-lying states on the  $^{10}\text{B} + \alpha$ -cluster states near the  $\alpha$ -decay should be checked in more sophisticated calculations that can reproduce well the low-energy spectra and the  $\alpha$ -decay threshold.

## ACKNOWLEDGMENTS

I thank Dr. Suhara for fruitful discussions. The computational calculations of this work were performed by using the supercomputers at YITP. This work was supported by the JSPS, KAKENHI Grant No. 26400270.

[1] W. von Oertzen, M. Freer, and Y. Kanada-En'yo, *Phys. Rep.* **432**, 43 (2006).  
 [2] Y. Kanada-En'yo and H. Horiuchi, *Prog. Theor. Phys. Suppl.* **142**, 205 (2001).  
 [3] Y. Kanada-En'yo, M. Kimura, and H. Horiuchi, *C. R. Phys.* **4**, 497 (2003).  
 [4] Y. Kanada-En'yo, M. Kimura, and A. Ono, *Prog. Theor. Exp. Phys.* **2012**, 01A202 (2012).

[5] H. Horiuchi, K. Ikeda, and K. Katō, *Prog. Theor. Phys. Suppl.* **192**, 1 (2012).  
 [6] Y. Fujiwara *et al.*, *Prog. Theor. Phys. Suppl.* **68**, 29 (1980).  
 [7] M. Seya, M. Kohno, and S. Nagata, *Prog. Theor. Phys.* **65**, 204 (1981).  
 [8] W. von Oertzen, *Z. Phys. A* **354**, 37 (1996); **357**, 355 (1997); **110**, 895 (1997).



- [9] K. Arai, Y. Ogawa, Y. Suzuki, and K. Varga, *Phys. Rev. C* **54**, 132 (1996).
- [10] A. Dote, H. Horiuchi, and Y. Kanada-En'yo, *Phys. Rev. C* **56**, 1844 (1997).
- [11] Y. Kanada-En'yo, H. Horiuchi, and A. Doté, *Phys. Rev. C* **60**, 064304 (1999).
- [12] N. Itagaki and S. Okabe, *Phys. Rev. C* **61**, 044306 (2000).
- [13] Y. Ogawa, K. Arai, Y. Suzuki, and K. Varga, *Nucl. Phys. A* **673**, 122 (2000).
- [14] Y. Kanada-En'yo, *Phys. Rev. C* **66**, 011303 (2002).
- [15] P. Descouvemont, *Nucl. Phys. A* **699**, 463 (2002).
- [16] M. Ito, K. Kato, and K. Ikeda, *Phys. Lett. B* **588**, 43 (2004).
- [17] M. Ito, *Phys. Lett. B* **636**, 293 (2006).
- [18] M. Freer *et al.*, *Phys. Rev. Lett.* **82**, 1383 (1999).
- [19] M. Freer *et al.*, *Phys. Rev. C* **63**, 034301 (2001).
- [20] A. Saito *et al.*, *Nucl. Phys. A* **738**, 337 (2004); *Mod. Phys. Lett. A* **25**, 1858 (2010).
- [21] N. Curtis, N. I. Ashwood, N. M. Clarke, M. Freer, C. J. Metelko, N. Soic, W. N. Catford, D. Mahboub, S. Pain, and D. C. Weissler, *Phys. Rev. C* **70**, 014305 (2004).
- [22] M. Milin *et al.*, *Nucl. Phys. A* **753**, 263 (2005).
- [23] M. Freer, E. Casarejos, L. Achouri, C. Angulo, N. I. Ashwood, N. Curtis, P. Demaret, C. Harlin, B. Laurent, M. Milin, N. A. Orr, D. Price, R. Raabe, N. Soic, and V. A. Ziman, *Phys. Rev. Lett.* **96**, 042501 (2006).
- [24] H. G. Bohlen, T. Dorsch, T. Kokalova, W. von Oertzen, C. Schulz, and C. Wheldon, *Phys. Rev. C* **75**, 054604 (2007).
- [25] N. Curtis *et al.*, *J. Phys. G* **36**, 015108 (2009).
- [26] Z. H. Yang *et al.*, *Phys. Rev. Lett.* **112**, 162501 (2014).
- [27] N. Soic, M. Freer, L. Donadille, N. M. Clarke, P. J. Leask, W. N. Catford, K. L. Jones, D. Mahboub, B. R. Fulton, B. J. Greenhalgh, D. L. Watson, and D. C. Weissler, *Phys. Rev. C* **68**, 014321 (2003).
- [28] W. von Oertzen *et al.*, *Eur. Phys. J. A* **21**, 193 (2004).
- [29] D. L. Price, M. Freer, N. I. Ashwood, N. M. Clarke, N. Curtis, L. Giot, V. Lima, P. McEwan, B. Novatski, N. A. Orr, S. Sakuta, J. A. Scarpaci, D. Stepanov, and V. Ziman, *Phys. Rev. C* **75**, 014305 (2007).
- [30] P. J. Haigh, N. I. Ashwood, T. Bloxham, N. Curtis, M. Freer, P. McEwan, D. Price, V. Ziman, H. G. Bohlen, T. Kokalova, C. Schulz, R. Torabi, W. von Oertzen, C. Wheldon, W. Catford, C. Harlin, R. Kalpakchieva, and T. N. Massey, *Phys. Rev. C* **78**, 014319 (2008).
- [31] T. Suhara and Y. Kanada-En'yo, *Phys. Rev. C* **82**, 044301 (2010).
- [32] M. Gai, M. Ruscev, A. C. Hayes, J. F. Ennis, R. Keddy, E. C. Schloemer, S. M. Sterbenz, and D. A. Bromley, *Phys. Rev. Lett.* **50**, 239 (1983).
- [33] P. Descouvemont and D. Baye, *Phys. Rev. C* **31**, 2274 (1985).
- [34] M. Gai, R. Keddy, D. A. Bromley, J. W. Olness, and E. K. Warburton, *Phys. Rev. C* **36**, 1256 (1987).
- [35] N. Furutachi, S. Oryu, M. Kimura, A. Dote, and Y. Kanada-En'yo, *Prog. Theor. Phys.* **119**, 403 (2008).
- [36] C. Fu, V. Z. Goldberg, G. V. Rogachev, G. Tabacaru, G. G. Chubarian, B. Skorodumov, M. McCleskey, Y. Zhai, T. Al-Abdullah, L. Trache, and R. E. Tribble, *Phys. Rev. C* **77**, 064314 (2008).
- [37] E. D. Johnson *et al.*, *Eur. Phys. J. A* **42**, 135 (2009).
- [38] W. von Oertzen *et al.*, *Eur. Phys. J. A* **43**, 17 (2010).
- [39] N. Curtis, D. D. Caussyn, C. Chandler, M. W. Cooper, N. R. Fletcher, R. W. Laird, and J. Pavan, *Phys. Rev. C* **66**, 024315 (2002).
- [40] N. I. Ashwood *et al.*, *J. Phys. G* **32**, 463 (2006).
- [41] S. Yildiz, M. Freer, N. Soic, S. Ahmed, N. I. Ashwood, N. M. Clarke, N. Curtis, B. R. Fulton, C. J. Metelko, B. Novatski, N. A. Orr, R. Pitkin, S. Sakuta, and V. A. Ziman, *Phys. Rev. C* **73**, 034601 (2006).
- [42] W. Scholz, P. Neogy, K. Bethge, and R. Middleton, *Phys. Rev. C* **6**, 893 (1972).
- [43] P. Descouvemont, *Phys. Rev. C* **38**, 2397 (1988).
- [44] G. V. Rogachev, V. Z. Goldberg, T. Lonroth, W. H. Trzaska, S. A. Fayans, K. M. Kallman, J. J. Kolata, M. Mutterer, M. V. Rozhkov, and B. B. Skorodumov, *Phys. Rev. C* **64**, 051302 (2001).
- [45] V. Z. Goldberg, *Phys. Rev. C* **69**, 024602 (2004).
- [46] M. Kimura, *Phys. Rev. C* **75**, 034312 (2007).
- [47] A. Tohsaki, H. Horiuchi, P. Schuck, and G. Ropke, *Phys. Rev. Lett.* **87**, 192501 (2001).
- [48] Y. Funaki, A. Tohsaki, H. Horiuchi, P. Schuck, and G. Ropke, *Phys. Rev. C* **67**, 051306 (2003).
- [49] T. Yamada and P. Schuck, *Phys. Rev. C* **69**, 024309 (2004).
- [50] Y. Funaki, T. Yamada, H. Horiuchi, G. Ropke, P. Schuck, and A. Tohsaki, *Phys. Rev. Lett.* **101**, 082502 (2008).
- [51] H. Morinaga, *Phys. Rev.* **101**, 254 (1956).
- [52] H. Morinaga, *Phys. Lett.* **21**, 78 (1966).
- [53] Y. Suzuki, H. Horiuchi, and K. Ikeda, *Prog. Theor. Phys.* **47**, 1517 (1972).
- [54] N. Itagaki, S. Okabe, K. Ikeda, and I. Tanihata, *Phys. Rev. C* **64**, 014301 (2001).
- [55] T. Ichikawa, J. A. Maruhn, N. Itagaki, and S. Ohkubo, *Phys. Rev. Lett.* **107**, 112501 (2011).
- [56] T. Suhara and Y. Kanada-En'yo, *Phys. Rev. C* **84**, 024328 (2011).
- [57] T. Mo and H. R. Weller, *Phys. Rev. C* **8**, 972 (1973).
- [58] Y. Kanada-En'yo, H. Morita, and F. Kobayashi, *Phys. Rev. C* **91**, 054323 (2015).
- [59] D. M. Brink, in *Proceedings of the International School of Physics: Enrico Fermi, Course 36*, edited by C. Bloch (Academic Press, New York, 1966).
- [60] A. B. Volkov, *Nucl. Phys.* **74**, 33 (1965).
- [61] N. Yamaguchi, T. Kasahara, S. Nagata, and Y. Akaishi, *Prog. Theor. Phys.* **62**, 1018 (1979); R. Tamagaki, *ibid.* **39**, 91 (1968).
- [62] F. Ajzenberg-Selove, *Nucl. Phys. A* **523**, 1 (1991).
- [63] A. Gallmann, F. Hibou, and P. Fintz, *Nucl. Phys. A* **123**, 27 (1969).
- [64] Y. Kanada-En'yo, T. Suhara, and Y. Taniguchi, *Prog. Theor. Exp. Phys.* **2014**, 073D02 (2014).